PHILOSOPHICAL TRANSACTIONS A

Phil. Trans. R. Soc. A.
doi:10.1098/not yet assigned

The influence of closed brine pockets and permeable brine channels on the thermo-elastic properties of saline ice

Aleksey Marchenko[1] and Ben Lishman[2,3]

[1]*The University Centre in Svalbard,P.O.Box 156,N-9171 Longyearbyen,Norway*
[2] *School of Engineering, London South Bank University, London SE10AA, UK*
[3]*Institute for Risk and Disaster Reduction, University College London, London WC1E6BT, UK*

Keywords: Saline ice, thermal expansion, thermo-elastic waves, permeability

Summary

A model of the thermo-elastic behaviour of saline ice is formulated, and model solutions describing thermo-elastic waves propagating into a half-space of the ice are investigated. The model is based on a proposal that saline ice is a matrix which encompasses both closed brine pockets and permeable channels filled with brine. Experiments on the thermal expansion of saline ice samples, and on thermo-elastic waves in saline ice, have been performed in the cold laboratories of the University Centre in Svalbard and in University College London. The experimental data are compared with theoretical conclusions. The experimental data support our hypothesis that the brine in saline ice is divided between closed pockets and open, permeable channels.

Introduction

Sea ice expands and contracts when its temperature changes. These volume changes can cause structural loads, and can induce thermal cracking, which makes the sea ice more fragile [1], and so understanding this behaviour can be important to a range of engineering and geophysical problems. Saline ice is a composite material – a solid ice matrix containing liquid and gas inclusions – and so understanding its thermal properties requires an understanding of the behaviour of the ice, brine, and air, and their interactions. The ice matrix itself is made up of pure ice grains (columns or platelets), and pockets and channels which contain brine and air. The ice is permeable, and the brine is able to migrate through the matrix under the influence of pressure gradients [2]. The permeability may be affected by thermal changes in the ice, as brine pockets separate and merge during freezing and melting cycles. Variations in permeability mean that sea ice may have material memory of thermal expansion and contraction, i.e. the current state may depend on previous conditions as well as current conditions.

Sea ice also exhibits unusual thermal expansion due to phase changes which occur in the matrix. Both fresh ice and brine exhibit typical thermal behaviour: they expand when heated and contract when cooled (i.e. their density decreases with increasing temperature). However, when brine freezes to form ice, this leads to a density reduction, since ice is less dense than water. When cooling leads to the freezing of brine, therefore, this can lead to a net density reduction: cooling in saline ice can cause expansion of the ice. The inverse can also occur, when warming of the saline ice causes brine to replace ice, leading to a reduction in volume. This behaviour was first discussed by Pettersson [3] and later studied experimentally and modelled by Malmgren [4].

*Author for correspondence (xxxx@yyyz.zz.zz).
†Present address: Department, Institution, Address, City, Code, Country

Malmgren assumed that all brine remained confined within the ice sample [4]. This is equivalent, within his formulation, to saying that the ice is impermeable. In his experiments, he immersed a sea ice sample in fluid and measured changes in fluid volume with temperature. He then used these total fluid volume changes to calculate thermal expansion coefficients. This experimental setup makes no allowance for the possibility that brine and air may be expelled into the confining fluid, and the confining fluid may be impelled into the ice [1]. In Malmgren's model, the volumetric effects of phase changes are entirely accommodated within the ice matrix, and therefore saline ice shows the atypical thermal properties discussed in the previous paragraph. In-situ observations [5] show that the average salinity of ice sheets remains virtually constant for the period of observations despite the prevalence of brine drainage networks and brine corrosion tubes that develop when the sheet warms.

Cox [6] revisited Malmgren's assumptions, and proposed that ice and brine are in fact free to expand and contract independently (this is equivalent to assuming that the ice is infinitely permeable). In Cox's formulation, phase changes are accommodated by brine drainage (or by brine being impelled into the ice) and so have no effect on the thermal expansion coefficient. He therefore proposes that the volumetric thermal expansion of saline ice is the same as that of fresh ice: around 1.5×10^{-4} K^{-1}. Cox's model and Malmgren's model therefore represent two ends of a spectrum which depends on sea ice permeability.

Later experiments give further insight. Johnson and Metzner [1] conducted a series of experiments on the linear thermal expansion of cylindrical ice samples taken from a sheet of first year congelation sea ice in Harrison Bay, Alaska. They used a Michelson Interferometer type Laser Dilatometer, along with a temperature control unit and computer-controlled data acquisition. They worked on two sets of samples, both with 38mm diameter: (a) 2ppt saline ice samples, 71.25mm long, and (b) 4ppt saline ice samples, 69.33mm long. To measure the samples with the dilatometer, they froze optically flat mirrors to microtomed sample surfaces. Their displacement resolution was 316.4nm, which corresponds to a strain resolution of 5×10^{-5}. They measured the thermal expansion coefficient to be very similar to the fresh ice thermal expansion coefficient of 1.5×10^{-4} K^{-1}. They concluded that their results supported the analysis of Cox [6].

Further systematic investigations were performed in the cold laboratories of the University Centre in Svalbard, Norway, and University College London, UK, from 2012-2015 [7-9]. These experiments used strain and temperature sensors based on fiber optics with Fiber Bragg Gratings (FBG). Fiber Bragg Gratings reflect light of certain wavelength, dependent on the extension of the grating. By measuring the wavelength of the reflected light, experimenters can determine the strain in the grating, and ultimately the temperature and strain in the ice sample. Thermal strains were measured with a sampling rate of 1Hz. The FBG system was designed by Advance Optic Solutions GmbH (Germany). In these experiments, the volumetric coefficient of thermal expansion was found to be close to 1.5×10^{-4} K^{-1} for fresh ice and ice with 2ppt salt. However, with 6ppt or higher salinity, negative values of thermal expansion were observed in several experiments.

The experiments show that the mean thermal expansion coefficient depends on temperature and salinity. They also show that thermal expansion coefficients vary around a mean, for a given temperature and salinity. The thermal expansion is observed to be a non-quasi-static process, where we assume that individual small deformations occur over time within the ice matrix, and these lead to changes in the thermal expansion over time. This suggests that modelling of thermal expansion should take into account temperature diffusion and liquid brine migration through the sample. A thermo-mechanical model of saline ice, accounting for migration of liquid brine through ice of finite, non-zero permeability, was proposed by Marchenko and Lishman [10]. The paper gave a theoretical model of the propagation of thermo-elastic waves, caused by temperature fluctuations at the ice surface, through an infinite half-space of saline ice. One conclusion was that temperature fluctuations and ice deformation are concentrated in a layer around 1cm from the surface when the period of the temperature fluctuations is around 10 minutes.

In the first part of the present paper we describe a thermo-mechanical model of saline ice incorporating both (a) closed pockets of liquid brine, and (b) permeable channels of liquid brine. We derive model solutions which describe the evolution of thermo-elastic waves in this ice. In the second part of the paper we describe experiments on the thermal expansion of saline ice samples, and on the propagation of thermo-elastic waves through these samples. In the conclusions we compare theoretical predictions to experimental results.

Model Equations

A model of sea ice brine distribution

In this paper, we assume that the brine contained in sea ice can be characterised in two ways: some fraction of the brine is contained in closed pockets, entirely surrounded by ice, while the remainder of the brine is in permeable channels. We assume that the amount of precipitated salt is very small and can be ignored. For sea ice, this is true when the ice temperature is higher than -8.2^{o}C [11]. We can then divide the sea ice matrix into two components:

- ***I**ce with **C**losed brine **P**ockets* (abbreviated to **ICP**). This fraction of the sea ice incorporates both the pure ice, and the brine held in impermeable pockets.
- *liquid **B**rine in **P**ermeable **C**hannels* (abbreviated to **BPC**).

This division is illustrated schematically in figure 1. This view allows us to describe observed Malmgren-like behaviour whilst simultaneously understanding sea ice as a permeable material.

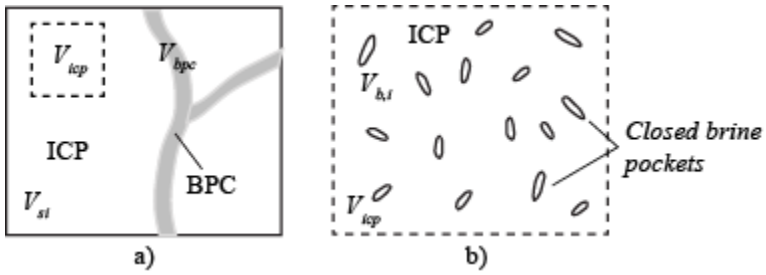

Figure 1. Model structures of saline ice (including brine in permeable channels BPC) (a) and the ice with closed brine pockets (ICP) (b).

In this section we explore the properties of this ice: how the mass and salt are distributed in the ice; how brine flows through the permeable channels; and how heat flows through the bulk ice. We then use this understanding to develop a model of thermo-elastic waves in sea ice: as the temperature at the surface of an ice sheet changes, how does the heat propagate through the ice, and how does the ice then deform? This model can then be directly compared to experimental results in the next section.

The proposed structural model of saline ice is similar to models describing the flow of partially molten rock through the Earth's convecting mantle, assuming viscous deformations of the permeable matrix (see, e.g., [12]). The details of the assumptions make a difference, with traditional models describing the flow of a low-viscosity fluid through a solid matrix (see, e.g., [13]). In case of saline ice the permeable matrix, the ICP, has strain-rate-dependent rheology (see, e.g., [14]). Within our approach the mass balance equations include a source term equal to the rate of mass transfer from matrix to melt (melting rate), and the permeability of the matrix changes with porosity depending on thermo-mechanical processes.

Mass Balance

We begin by defining the volumetric concentrations (or volume fractions) of each component in a unit volume of sea ice. The volumetric concentration of BPC (v_b) in the volume of saline ice V_{si} shown in Fig. 1a is equal to V_{bpc}/V_{si}, where V_{bpc} is the BPC volume. The volumetric concentration of ICP (v_{icp}) is equal to the ratio $(V_{si}\text{-}V_{bpc})/V_{si}$, where $V_{si}\text{-}V_{bpc}$ is the volume of ICP in the saline ice volume V_{si}, and therefore

$$v_{icp} + v_b = 1 \qquad (1)$$

which is the same as saying that the entire volume of sea ice is composed of either ICP or BPC. The ratio of ICP to BPC may change with temperature.

ICP is made up of ice and brine only: we denote the volume fractions of ice and brine in ICP as v_i and v_{bi} respectively (Fig. 1b), such that

$$v_i + v_{bi} = 1 \qquad (2)$$

ICP is not permeable by brine. Temperature changes will affect the ratio of v_i and v_{bi}. The quantity v_{bi} – the brine fraction in ICP – will never fall to zero since the increasing brine salinity will eventually prevent freezing. A decrease in v_b may lead to a transformation from BPC to a chain of closed pockets if the temperature is sufficiently low.

The sea ice density can be determined from the densities and volume fractions of its constituent parts:

$$\rho_{si} = \rho_{icp} v_{icp} + \rho_b v_b \tag{3}$$

Salt Balance

The salinity of sea ice can be determined using the formula

$$\rho_{si}\sigma_{si} = \rho_{icp} v_{icp}\sigma_{icp} + \rho_b v_b \sigma_b \tag{4}$$

where σ represents salinity (this equation states that the mass of salt per unit volume of sea ice is equal to the mass of salt in ICP in that unit volume plus the mass of salt in BPC in that volume).

We assume that the liquid brine and pure ice are in thermodynamic equilibrium, and therefore the salinities (and hence densities) of the brine in closed pockets and of brine in permeable channels are the same. Therefore the ICP salinity can be determined as follows

$$\rho_{icp}\sigma_{icp} = \rho_b v_{bi}\sigma_b \,. \tag{5}$$

Shwerdtfeger [11] gives the density of ice containing brine as equation 2.3.1. Adapting this for ICP, we find

$$\rho_{icp} = \frac{\rho_b \rho_i \sigma_b}{\rho_i \sigma_{icp} + \rho_b(\sigma_b - \sigma_{icp})} \tag{6}$$

Pure ice density depends on the temperature, and is given by the formula [15]

$$\rho_i \approx \frac{916.8}{1+\alpha_i T}(\mathrm{kg/m^3}) \tag{7}$$

The volumetric coefficient of thermal expansion $\alpha_i = 1.53\cdot 10^{-4}\mathrm{K}^{-1}$. The density of brine (and hence of BPC) is also given by Schwerdtfeger [11]:

$$\rho_b = \rho_w(1+S) \tag{8}$$

where ρ_w is the density of pure water and S is the fractional salt content of the brine,

$$\begin{aligned} S &= -0.0182\cdot T\,, & T &> -8.2^\circ\,\mathrm{C} \\ S &= 0.149 - 0.01\cdot(T+8.2)\,, & T &\in (-23^\circ\mathrm{C}, -8.2^\circ\mathrm{C}) \end{aligned} \tag{9}$$

(The fractional salt content is related to the salinity by $\sigma = S/(1+S)$, and hence σ_b can also be calculated as a function of temperature).

To recap: given the temperature, we can find from formulas (8) and (9) the density and salinity of the brine everywhere in the ice, as well as the pure ice density from formula (7). If we then knew the ICP salinity we could calculate the density of ICP from (6) and the volume fraction of brine in ICP from (5). This would allow us to calculate the ice density and the volumetric concentration of ICP from (3) and (4)

$$\rho_{si} = \rho_{icp}(\sigma_b - \sigma_{icp})\Delta^{-1},\ v_{icp} = (\sigma_b - \sigma_{si})\Delta^{-1},\ \Delta = \sigma_b - \sigma_{si} + \rho_{icp}(\sigma_{si} - \sigma_{icp})/\rho_b \tag{10}$$

Overall, then, in our formulation, the bulk temperature, and ice and ICP salinities are sufficient to define all densities and volume fractions.

Thermal expansion of ICP

A change of ICP mass may occur due to brine transfer between ICP and BPC, and can be related to a change of the ICP salinity by the formula

$$\delta m_{icp} = V_{icp}(\partial\rho_{icp} / \partial\sigma_{icp})\delta\sigma_{icp} \qquad (11)$$

where $m_{icp}=\rho_{icp}V_{icp}$ is the mass of an ICP particle with volume V_{icp}. In the case when mass change is caused by temperature change, from (11), it follows that

$$\frac{d(\rho_{icp}V_{icp})}{dT}\delta T = V_{icp}\frac{\partial\rho_{icp}}{\partial\sigma_{icp}}\frac{\partial\sigma_{icp}}{\partial T}\delta T \qquad (12)$$

The volumetric coefficient of thermal expansion of ICP is determined by the formula

$$\alpha_{icp} = \frac{1}{V_{icp}}\frac{dV_{icp}}{dT} \qquad (13)$$

From (12) and (13) we find the standard formula for the calculation of the volumetric coefficient of thermal expansion of ICP:

$$\alpha_{icp} = -\frac{1}{\rho_{icp}}\frac{d\rho_{icp}}{dT}\bigg|_{\sigma_{icp}=const} \qquad (14)$$

System dynamics

The mass balance of the BPC is formulated as

$$\frac{\partial(\rho_b\nu_b)}{\partial t} + \nabla\cdot\left(\rho_b(\mathbf{v}_b + \mathbf{v}_{icp})\nu_b\right) = \rho_b\frac{\partial\nu_b}{\partial t},\ \nabla = \left(\frac{\partial}{\partial x},\frac{\partial}{\partial y},\frac{\partial}{\partial z}\right) \qquad (15)$$

where t is the time, x, y, and z are the spatial coordinates, $\mathbf{v}_b$ is the BPC velocity relatively the ICP and $\mathbf{v}_{icp}$ is the ICP velocity in an absolute frame reference. The term $\rho_b\partial\nu_b/\partial t$ is the source or sink of the brine due to the ice melting, brine refreezing and brine exchange with the ICP.

The momentum balance, and hence velocity, of BPC is given by Darcy's law:

$$\nu_b\mathbf{v}_b = -k_{si,b}\mu_b^{-1}\nabla p \qquad (16)$$

where $k_{si,b}$ is the permeability of sea ice by brine, μ_b=1.8·10^{-3} Pa·s is the dynamic viscosity of water, and p is the pressure in the brine channels. The permeability of saline ice by brine is determined by the formula

$$k_{si,b} = k_{si,b0}e^{15\sqrt{\nu_b}} \qquad (17)$$

where the coefficient $k_{si,b0}=10^{-13}$ m^2 characterizes ice permeability at low values of the liquid brine content. Formula (17) approximates the data of the laboratory and numerical simulations shown in Fig. 2 in [16].

We assume that ice deformations are sufficiently slow and inertial effects can be ignored. The equations of static equilibrium based on Hooke's law can then be used, assuming an elastic model for the ice (i.e. for small displacements and short term effects) [17]:

$$\nabla \cdot \boldsymbol{\sigma}_d = \nabla p_{icp} \tag{18}$$

$$\boldsymbol{\sigma}_d = 2G\boldsymbol{\varepsilon}_d\,,\ -p_{icp} = \mathrm{K}\varepsilon_{icp} - \mathrm{K}\alpha_{icp}(T - T_0) \tag{19}$$

where p_{icp} is the ICP pressure, $\boldsymbol{\sigma}_d$ and $\boldsymbol{\varepsilon}_d$ are the deviators of stresses and strains, ε_{icp} is the volumetric strain, G = 3.5 GPa and K = 8.9 GPa are the shear modulus and the bulk modulus of ice [18], α_{icp} is the volumetric coefficient of thermal expansion of the ICP, and T_0 is a reference temperature. Equation (18) describes a static momentum balance in ICP, and formulas (19) describe Hooke's law for thermo-elastic materials. Formulas (19) would need to be modified to describe ice creep and delayed elasticity if long-term processes are considered. The strain rate deviator is related to the ICP velocity by standard formulas specifying strain rates in continuum mechanics (see, e.g., [17]).

The energy balance is given by the heat transfer equation [19, 20]

$$\left\langle \rho c \right\rangle_{si} \frac{dT}{dt} + \rho_i L_i \frac{\partial(\nu_b + \nu_{icp}\nu_{bi})}{\partial t} = \nabla \cdot \left(\lambda_{si} \nabla T\right) - \mathrm{K}\,\nu_{icp}\alpha_{icp}(T - T_0)\nabla \cdot \mathbf{v}_i + 2\nu_b \mu_b \mathbf{e}_b \cdot \mathbf{e}_b\,, \tag{20}$$

where the material derivative is expressed by the formula $d/dt = \partial/\partial t + \nu_b \mathbf{v}_b \cdot \nabla$, and the coefficients of specific heat capacity and thermal conductivity are calculated by the formulas

$$\left\langle \rho c \right\rangle_{si} = \rho_i c_i \nu_i \nu_{icp} + \rho_b c_b (\nu_b + \nu_{bi}\nu_{icp})\,,\ \lambda_{si} = \lambda_i \nu_i \nu_{icp} + \lambda_b (\nu_b + \nu_{bi}\nu_{icp})\,. \tag{21}$$

Here c_i and c_b are the specific heat capacities, and λ_i and λ_b are the thermal conductivities of ice and brine, L_i=333.4 kJ/kg is the latent heat of ice, $\mathbf{e}_b$ represents the strain rates of the brine. The second term on the left hand side of equation (20) describes the latent heat rate due to the brine freezing or ice melting. The last two terms on the right hand side of equation (20) are related to the heat produced due to the thermal expansion of ice and due to viscous energy dissipation in the brine.

Further it is assumed that the specific heat capacity and thermal conductivity of brine are equal to the specific heat capacity and thermal conductivity of water. The specific heat capacities and thermal conductivities of ice and water are given by the formulas [11]

$$c_w = 4.23\,\mathrm{kJ/(kg^\circ C)}\,,\ c_i = 2.12\,\mathrm{kJ/(kg^\circ C)}\,,\ \lambda_w = 0.58\,\mathrm{W/(m^\circ C)}\,,\ \lambda_i = 2.24\,\mathrm{W/(m^\circ C)} \tag{22}$$

The time-varying salt balance in the ice is written in the form

$$\partial\left(\rho_{si}\sigma_{si}\right)/\partial t + \nabla \cdot \left(\rho_b \sigma_b (\mathbf{v}_b + \mathbf{v}_{icp})\nu_b + \rho_{icp}\sigma_{icp}\mathbf{v}_{icp}\nu_{icp}\right) = 0 \tag{23}$$

The term $\rho_b \sigma_b \nu_b$ is equal to the mass of salt in BPC per unit volume of sea ice, and the term $\rho_b \sigma_b \nu_b \mathbf{v}_b$ is equal to the salt flux.

Three scalar equations describing balance of mass (15), energy (20) and salts (23), and two vector equations describing momentum balance in PBC (16) and ICP (18) form a system for the calculation of three scalar variables (p, T and σ_{si}) and two velocity vectors ($\mathbf{v}_b$ and $\mathbf{v}_{icp}$). The model is not complete since equations describing brine exchange between ICP and BPC are not formulated. We assume that the brine exchange can be described by an empirical dependence

$$\sigma_{icp} = \sigma_{icp}(\sigma_{si}, T) \tag{24}$$

Further we investigate this dependence using data from laboratory experiments on the thermal expansion of saline ice and on measurement of thermo-elastic waves in saline ice.

Thermo-elastic waves in saline ice

In experiments described later in this paper, we measure the thermal expansion of sea ice as temperature changes propagate through the ice. In order to describe these experiments, we develop our model of saline ice to describe thermo-elastic waves propagating into an ice half-space.

If the temperature of the upper surface of an ice sheet changes, then these temperature changes propagate down into the ice sheet, over time and with damping. Stresses due to these temperature changes also propagate, and, in the case of saline ice, may cause brine migration. This complicated interplay is modelled in this section of the paper. It is assumed that the steady state of a saline-ice-filled half space $x > 0$ is described by the following characteristics:

$$p = 0,\ T = T_0,\ \sigma_{si} = \sigma_{si0},\ \sigma_{icp} = \sigma_{icp0},\ \mathbf{v}_{icp} = \mathbf{v}_b = 0 \qquad (25)$$

We are then interested in the fluctuations around this steady state. Let us consider deformations of a saline ice half-space (x>0) initiated by small temperature variations around T=T_0 at x=0

$$T = T_0 + \delta T,\ \delta T = A_T \cos \omega t,\ x = 0 \qquad (26)$$

where A_T is the amplitude and ω is the frequency of the temperature wave at the ice surface.

We investigate the evolution of saline ice characteristics caused by periodical variations of the temperature at the surface described by formulas (26) and assume that the saline ice characteristics depend on the time t and spatial variable x, and are represented as follows

$$\mathbf{X} = \mathbf{X}_0 + \delta\mathbf{X} \qquad (27)$$

Each component of vector **X** represents some characteristic of the saline ice, and each component of vector δ**X** represents a perturbation of the ice characteristic near its value at the steady state specified by vector $\mathbf{X}_0$, according to the formulas

$$\mathbf{X}_0 = (p = 0, T_0, \sigma_{si0}, \sigma_{icp0}, v_{ix} = 0, v_b = 0),\ \delta\mathbf{X} = (\delta p, \delta T, \delta\sigma_{si}, \delta\sigma_{icp}, \delta v_{ix}, \delta v_b) \qquad (28)$$

where v_{ix} and v_b are the velocities of ICP and BPC in the x direction. Components of the vector $\mathbf{X}_0$ are background characteristics of ice. In this paper we use the subscript "0" to denote variables calculated using the background characteristics of ice.

A set of equations used for the investigation of the temporal and spatial evolution of δ**X** is specified further in the case when all variables depend only on the time t and spatial coordinate x. In this case nonzero components of the ICP strain rate and vertical displacement are determined by the formulas

$$\delta e_{icp} = \frac{\partial \delta v_{ix}}{\partial x},\ \delta v_{ix} = \frac{\partial \delta u_{ix}}{\partial t} \qquad (29)$$

From Darcy's law (16) it follows

$$v_{b0}\delta v_b = -\frac{k_{si,bo}}{\mu_b}\frac{\partial \delta p}{\partial x}, \qquad (30)$$

Substitution of (30) into equations (15) and (23) – the mass balance of BPC and the salt balance - and linearization leads to the equations

$$\rho_{b0,T}\frac{\partial \delta T}{\partial t}+\rho_{b0}\delta e_{icp}=\gamma_{b0}\frac{\partial^2 \delta p}{\partial x^2},\ \gamma_{b0}=\frac{\rho_{b0}k_{si,b0}}{\mu_b} \tag{31}$$

$$\sigma_{si0}\frac{\partial \delta \rho_{si}}{\partial t}+\rho_{si0}\frac{\partial \delta \sigma_{si}}{\partial t}+(\rho_b\sigma_b v_b+\rho_{icp}\sigma_{icp}v_{icp})_0\delta e_{icp}=(\sigma_b v_b\gamma_b)_0\frac{\partial^2 \delta p}{\partial x^2} \tag{32}$$

where the ice density perturbation $\delta\rho_{si}$ is, according to the first part of formula (10), a linear function of δT, $\delta\sigma_{si}$ and $\delta\sigma_{icp}$

$$\delta\rho_{si}=\left(\frac{\partial\rho_{si}}{\partial T}+\frac{\partial\rho_{si}}{\partial\sigma_{icp}}\frac{\partial\sigma_{icp}}{\partial T}\right)_0\delta T+\left(\frac{\partial\rho_{si}}{\partial\sigma_{si}}+\frac{\partial\rho_{si}}{\partial\sigma_{icp}}\frac{\partial\sigma_{icp}}{\partial\sigma_{si}}\right)_0\delta\sigma_{si} \tag{33}$$

The heat transfer equation (20) is written after linearization as follows

$$\langle\rho c\rangle_{si0}\frac{\partial\delta T}{\partial t}+\rho_{i0}L_i\frac{\partial(\delta v_b+v_{icp0}\delta v_{bi})}{\partial t}=\lambda_{si0}\frac{\partial^2\delta T}{\partial x^2} \tag{34}$$

where according to formulas (1,5,6,10) the perturbations δv_b and δv_{bi} are linear functions of δT, $\delta\sigma_{si}$ and $\delta\sigma_{icp}$.

$$\delta v_b=-\left(\frac{\partial v_{icp}}{\partial T}+\frac{\partial v_{icp}}{\partial\sigma_{icp}}\frac{\partial\sigma_{icp}}{\partial T}\right)_0\delta T-\left(\frac{\partial v_{icp}}{\partial\sigma_{si}}+\frac{\partial v_{icp}}{\partial\sigma_{icp}}\frac{\partial\sigma_{icp}}{\partial\sigma_{si}}\right)_0\delta\sigma_{si} \tag{35}$$

$$\delta v_{bi}=\left(\frac{\partial v_{bi}}{\partial T}+\frac{\partial v_{bi}}{\partial\sigma_{icp}}\frac{\partial\sigma_{icp}}{\partial T}\right)_0\delta T+\left(\frac{\partial v_{bi}}{\partial\sigma_{si}}+\frac{\partial v_{bi}}{\partial\sigma_{icp}}\frac{\partial\sigma_{icp}}{\partial\sigma_{si}}\right)_0\delta\sigma_{si}$$

Equations (18) and (19) are differentiated with respect to time and reduced to one equation

$$\left(\frac{4G}{3}+\mathrm{K}\right)\delta e_{icp}=\mathrm{K}\alpha_{icp}\frac{\partial\delta T}{\partial t} \tag{36}$$

The perturbation of the ICP salinity is described according to equations (24) as follows

$$\delta\sigma_{icp}=\left(\frac{\partial\sigma_{icp}}{\partial T}\right)_0\delta T+\left(\frac{\partial\sigma_{icp}}{\partial\sigma_{si}}\right)_0\delta\sigma_{si} \tag{37}$$

Six equations (30-32), (34), (36) and (37) form a closed system describing the evolution of the vector $\delta\mathbf{X}$ specified by the second formula (28). We consider the solution in the form

$$\delta\mathbf{X}=\mathrm{Re}\left[\mathbf{A}e^{i(\omega t+kx)}\right],\ \mathbf{A}=A_T\left(a_p,1,a_{\sigma si},a_{\sigma icp},a_{vix},a_{vb}\right) \tag{38}$$

where the products of the temperature amplitude A_T on the coefficients a_p, $a_{\sigma si}$, $a_{\sigma icp}$, a_{vix} and a_{vb} are the perturbation amplitudes of the BPS pressure, ice salinity, ICP salinity, ICP velocity and BPC velocity. Substitution of (37) in equations (31)-(36) leads to a system of five linear algebraic equations with respect to five components of the vector **A**. This homogeneous system has a nontrivial solution when the determinant is equal to zero. The last condition is called the dispersion equation of thermo-elastic waves (TEW):

$$\omega=ik^2/X_T, \tag{39}$$

where X_T is given in formulas (42) in the section Additional information. The dispersion equation is a rule for the calculation of the wave number k corresponding to a given wave frequency ω. If ω and k satisfy the dispersion equation, then all numbers a_p, $a_{\sigma si}$,a_{vix} and a_{vb} are calculated from equations (30-32), (34) and (36), while the amplitude A_T remains an arbitrary quantity. From equation (39) it follows that the wave number is a complex quantity, i.e. it is the sum of a real part describing periodical oscillations of ice characteristics in the direction of wave propagation and an imaginary part describing the damping of wave amplitude. Similar dispersion equations describe pure thermal waves caused by temperature oscillations at the surface of materials, and Stokes waves in viscous fluids caused by the oscillations of shear displacements at the surface (see, e.g., [20]).

Numerical estimates using formulas (42) show very little dependence of X_T from $\partial\sigma_{icp}/\partial T$, when $\sigma_{si}< 10$ ppt, $\sigma_{icp}< \sigma_{si}$, $T\hat{I}$ (-8,-2)^{o}C, and $\partial\sigma_{icp}/\partial T$ is approximated by the linear dependence $\partial\sigma_{icp}/\partial T\approx-\sigma_{icp}/6$ constructed according to the temperature range. Therefore we neglect all terms proportional to $\partial\sigma_{icp}/\partial T$ when processing experimental data. In our experiments (described below) we didn't observe significant changes of the ice salinity. Therefore in the analysis of the experimental results we also neglect all terms proportional to $\partial\sigma_{si}/\partial T$.

The amplitude of vertical displacement of the ice surface is then equal to

$$A_u = -\frac{i}{k}\frac{\mathrm{K}\alpha_{icp0}}{4G/3+\mathrm{K}}A_T \qquad (40)$$

The amplitudes A_u and A_T can be measured in experiments. Their absolute ratio $|A_u/A_T|$ (hereafter named the DT ratio, or displacement-temperature ratio) depends on the ice characteristics and wave frequency. The model given can be adapted to describe experimental data by varying the background characteristics ν_{b0}, ν_{bi0} or σ_{icp}. From equations (31) and (32) it follows that only pore pressure amplitude a_p depends on the ice permeability $k_{si,b0}$. According to formula (40) the amplitude of vertical displacement of the ice surface A_u is proportional to the amplitude of surface temperature A_T, the square root of the period of the temperature oscillations $\sqrt{(2\pi/\omega)}$ and other characteristics of saline ice excluding the ice permeability. Experimental data can therefore be used to test the validity of the structural model above, using equation (40), and also to infer parameters which are not well known: for example the ICP salinity σ_{icp}.

Experimental Investigations

Thermal expansion of unconfined saline ice

Experiments on thermal expansion of unconfined samples of fresh and saline ice were performed in the cold laboratory of the University Centre in Svalbard (UNIS) [7,8]. The ice samples had a rectangular shape, with the long dimension around 20cm and the shorter dimensions 5-10cm. The optical fibers with FBG strain sensors had an integrative working length of 20cm that was defined by two brass anchor bolts with nuts and washers. The optical fibers were placed into 2mm-wide cuts that were sawn in the ice samples, and were fastened at the edges of the ice samples with nuts and washers (Fig.2a). The ice block's thermal expansion or shrinkage is therefore transferred to the optical fiber with the FBG inside (this fiber is prestrained to around 0.3% by adjusting the nuts accordingly). The FBG fiber was not frozen into place, since this would allow localized shear around the FBG itself to distort the measurements. The FBG temperature sensor (thermistor string) was encapsulated in a 1mm stainless steel capillary tube and inserted into a drilled hole in the ice sample, next to the FBG strain sensor.

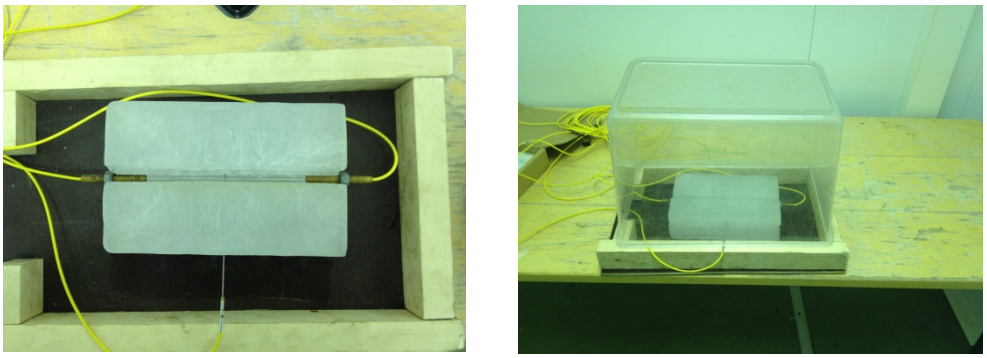

a) b)

Figure 2. Installation of FBG strain sensor and thermistor string in ice sample (a). Ice sample inside plastic housing (b).

The equipment used in our measurement setup includes a broadband LED light source with a central wavelength of 1550nm and a bandwidth (FWHM) or ~90nm (AOS GmbH, Germany), a NIR spectrometer 'I-MON 512E-USB 2.0 interrogation monitor' with a detectable spectral width of 1510-1595nm (Ibsen Photonics S/A, Denmark), a PC, and two FBG sensors, one for strain measurement and one for temperature measurement (both AOS GmbH, Germany). The Ibsen monitor is distributed with operating software, including a LabView source code. The experimental schematic is shown in Fig.3a. All electronic devices – the LED source, the spectrometer, and the PC – were installed outside the cold laboratory. Regular optical single-mode cables were used to connect the equipment to the FBG sensors embedded into the ice sample in the cold laboratory.

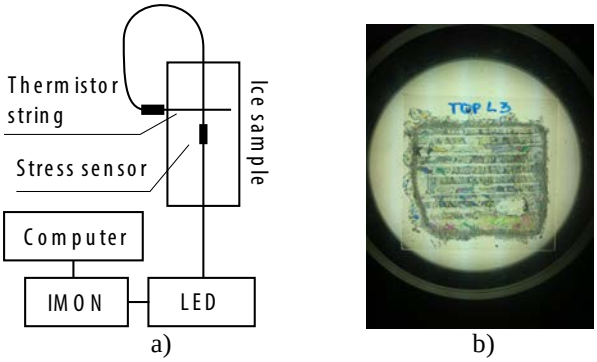

a) b)

Figure 3. Schematic of experiment for measuring of thermal expansion (a), and thin vertical section of laboratory ice used in the tests (b).

The ice sample was covered by a plastic housing to avoid evaporation (Fig.2b). The temperature in the cold laboratory (2.5x2.5x1.8m) was changed in increments of 2°C from -20° C to a nominal 0° C, programmed and displayed on the laboratory's control system. Measurements of actual temperature in the cold laboratory show temperature oscillations with amplitude about 1.8°C across a range of mean temperature. The period of this temperature oscillation (when the room temperature was programmed to be constant) was 12 min. During the experiment, we realized that the actual air temperature close to the ice samples was lower than the displayed temperature by several degrees. Temperature and extension are measured at 1 sample/s.

A representative time of temperature equilibration over a sample is estimated by the formula $t^*=\rho_{si}c_{si}l_0^2/\lambda_{si}$, where ρ_{si}=920 kg/m^3 is typical value of sea ice density, λ_{si}= 2 W/(m·K) is a typical value of the thermal conductivity of sea ice, l_0=0.1 m is representative length of the sample, and c_{si} is the specific heat capacity of saline ice. The time taken for temperature to equilibrate in fresh ice samples is estimated at 2.5 hours when c_{si} is equal to the specific heat capacity of fresh ice: 2 kJ/(kg·K). Because of the phase changes around brine pockets the specific heat capacity of saline ice can be much greater than the specific heat capacity of fresh ice [11]. Therefore time intervals for the temperature increments were set to 2-3 hours or greater.

A mixture of sea water, pumped from a nearby fjord, and fresh water was used to prepare saline ice samples. The salt water was added to a rectangular vessel and allowed to freeze layer by layer. The thickness of each layer was about 1 cm.

Fresh ice samples were frozen by the same method from fresh water. The lab-grown saline ice had a columnar structure in each horizontal layer with clear boundaries between the layers (Fig.3b). The salinity of the ice samples was measured before and after the experiments with a Mettler Toledo Seven Pro conductivity meter SG7, with resolution 0.01ppt. Multiple 'dummy' samples were kept under the same conditions as the strain-gauged sample: these samples were then used to measure changes in salinity and density during the experiments. To measure ice density we measure sample weight and sample volume. The volume measurement was performed by submerging the ice sample in a graded tube filled with oil with a density smaller the ice density. The sample volume is taken as equivalent to the volume of oil displaced. Table 1 shows the salinity and density variations, measured twice per day, when the room temperature changed between -5°C and -15°C with one closed cycle per day. One can see that the laboratory ice salinity remained similar over the four day experiment. The mean value of the ice density is 904 kg/m^3. The gas content, estimated with air temperature -8°C and ice salinity 6 ppt, is about 2.4 % [14].

Table 1. Temporal variations of the salinity of ice samples under cyclic temperature change.

Day	Time	Ice salinity, ppt	Ice density, kg/m^3
1	19:00	6.1	867
2	10:00	6.2	889
2	14:00	6.6	960
3	10:00	6.2	914
3	14:00	6.1	884
4	13:00	6.0	912

From the experimental data we calculate the effective coefficient of linear thermal expansion (ECTE) with the formula

$$\alpha_{lsi}(T) = \frac{1}{L}\frac{\Delta L}{\Delta T}, \tag{41}$$

where $\Delta L/L$ is the lengthening or shortening of ice samples measured with the FBG strain sensor when the ice temperature changes from T to $T+\Delta T$. The ECTE describes measured properties of ice samples.

The coefficient of linear thermal expansion (CTE) is a material property, while ECTE is a characteristic of thermal expansion measured in the experiment. We consider saline ice as an isotropic material and assume that the coefficient of linear thermal expansion is one third of the coefficient of volumetric thermal expansion. The linear coefficient of thermal expansion of fresh ice (CTEFI) is equal $\alpha_{li}=\alpha_i/3=5.1\times10^{-5}\mathrm{K}^{-1}$. Results of the tests with fresh ice samples are shown in Fig. 4. Figure 4a shows temperature variations in the ice samples as measured with the FBG thermistor string. The insert graph in Fig. 4a shows temporal variations induced by the cooling cycle of the fans. The data are averaged over 15 min intervals to minimize the influence of the fan cycle. Calculated values for the ECTE for fresh ice are shown in Fig. 4b, and these are close to the CTEFI, shown by the dashed line.

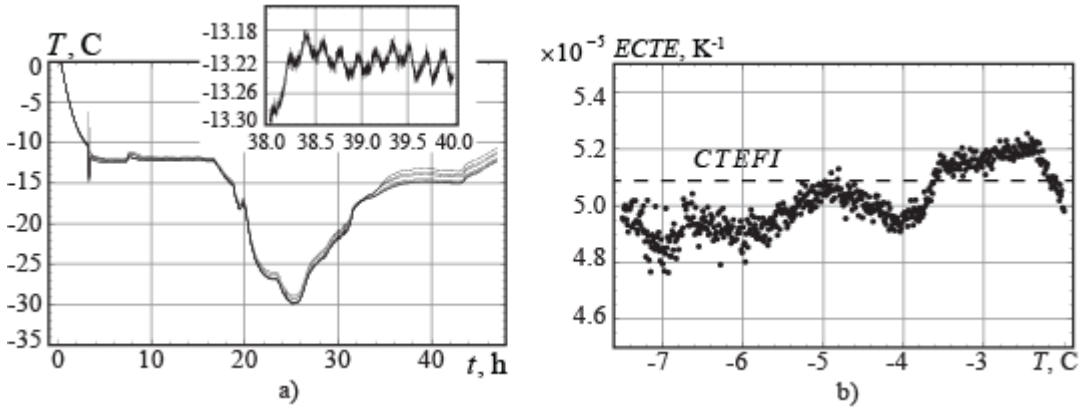

Figure 4. Temperature (a) and the coefficient of thermal expansion versus the time (b), for fresh ice sample in long-term test.

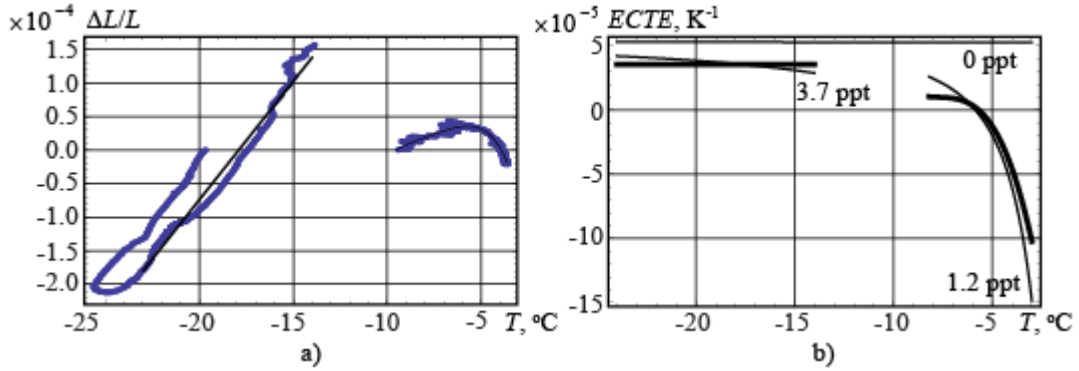

Figure 5. Dependencies of ice sample extension versus the ice temperature measured in the experiment (blue lines) and their polynomial interpolations (black lines) (a). ECTE versus the ice temperature calculated from the polynomial interpolations of the experimental data (thick lines) and theoretical dependencies of CTE on temperature, calculated with adjusted values of the ice salinity σ_{icp} .

Figure 5 shows the results of a test with ice sample salinity 6ppt. Blues lines in Fig. 6a correspond to the values of the ice sample extension and temperature measured in the experiment. Black lines in Fig. 5a show polynomial interpolations of the experimental data. Thick lines in Fig. 5b show ECTE versus the temperature calculated using the polynomial interpolation of the experimental data. Thin lines in Fig. 5b show theoretical dependencies of CTE on temperature, calculated with adjusted values of the ice salinity σ_{icp} are calculated from formula (14) with using formulas (6-10). The test shows thermal expansion similar to that described by Malmgren [4], with a negative ECTE, when the ice temperature is higher than -8°C. Formula (11) gives a good approximation of the experimental results with σ_{icp}=3.7 ppt when the ice temperature is less than -14 °C, and with σ_{icp}=1.2 ppt when the ice temperature is higher than -8 °C. We explain the observed decrease of the ECTE in warm ice the variation in the amount of brine trapped in closed pockets. This amount is estimated about 60% of total brine content when the ice temperature is below -14 °C, and about 20% of total brine content when the ice temperature is above -8 °C.

Thermal expansion of constrained saline ice

A series of experiments were undertaken in the cold rooms of University College London [9]. The FBG strain sensor was used to measure the linear strain in ice samples of cylindrical shape constrained between two steel pipes. The initial intent of this experiment was to investigate slip between ice and steel during thermal expansion and contraction. The ice was formed between two steel pipes: an outer pipe with inside diameter 11cm, and an inner pipe with outside diameter 2cm (see figure 6). Fresh ice was made from London tap water; saline ice from the same, with 8ppt NaCl added. The samples were formed in layers, so that up to 1cm depth of water was added and allowed to freeze before the next layer was formed. No evidence was seen of supercooled water or large bubbles within these layers. The outer pipe has length 180mm, and the samples are milled 5mm from either end of the pipe, such that the initial ice sample has two flat parallel ends 190mm apart. On these flat ends we place an aluminium spacer of width 4mm which supports the FBG strain sensor such that expansion in the ice in the along-pipe direction stretches the sensor.

Temperatures are measured using the FBG 12-thermistor string inserted through a drilled hole in the ice (or ice and pipe), such that temperatures are recorded through the sample in the horizontal direction. The temperature used for calibration of the strain sensor is that closest to the sensor. For calculation of thermal expansion, we use the average of thermistors located inside the ice sample, which gives a mean value through the ice, but eliminates the thermistors in the air, which respond much faster to temperature changes in the room. Temperature and extension are measured at 1 sample/s. The entire apparatus is shown in a photograph and schematic in Fig. 6.

Figure 7a shows strain, as a function of temperature, measured at two different stages of a single experiment. Figure 7b shows this strain-temperature relationship expressed as ECTE. Measurements of thermal expansion are taken during periods when the temperature variation in the ice is greater than 0.1°Cs^{-1} (i.e. only when the temperature gradient is sufficiently large). Two clusters of results are visible in Fig. 7, and marked as 1 and 2. This split set of results is derived from one single experiment. The two clusters represent two different stages of the experiment, around 24h apart, and separated by cooling the ice to -16°C: the more negative values of ECTE (i.e. cluster 1) come from the first stage of the experiment, and the values close to zero (cluster 2) from a later stage of the experiment. In both clusters the ice was warming as measurements were taken. In cluster 1 the ice clearly contracts with increasing temperature, whereas in cluster 2 the ice expands with increasing temperature up to around -7°C, then contracts. It is surprising that the same ice, during the same experiment, shows such variation in ECTE against temperature. We note that the constrainment of the ice

means the ECTE could take values between the volumetric and linear coefficients of thermal expansion, but this switching between the volumetric and linear expansion doesn't explain the two regions of ECTE in the temperature range from -10° C to -6 ° C. It is possible that the constraining pipes cause some brine regions to switch over time between BPC and ICP, but this effect needs further investigation.

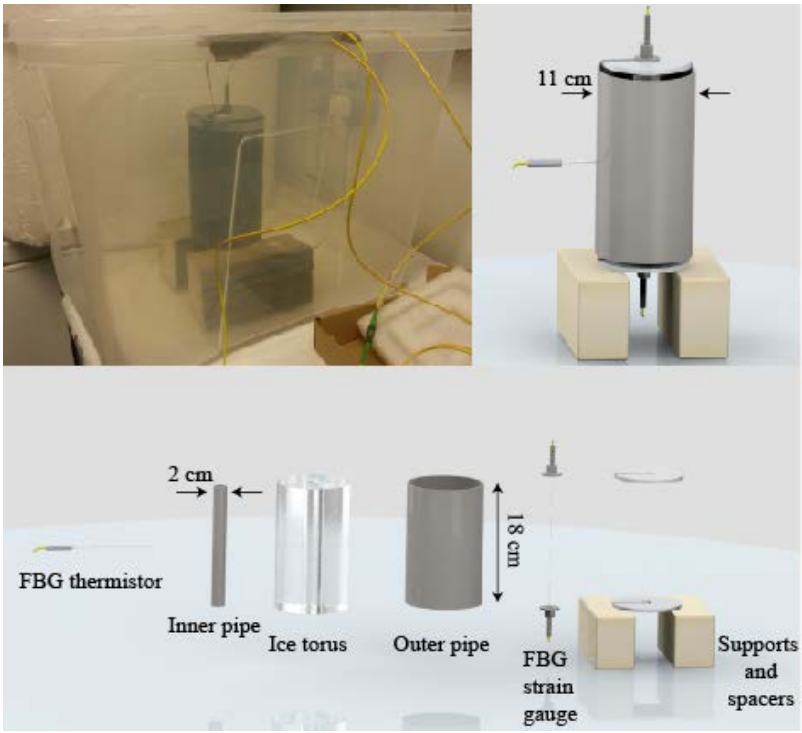

Figure 6. Full constrained-sample experiment photo, schematic and exploded schematic.

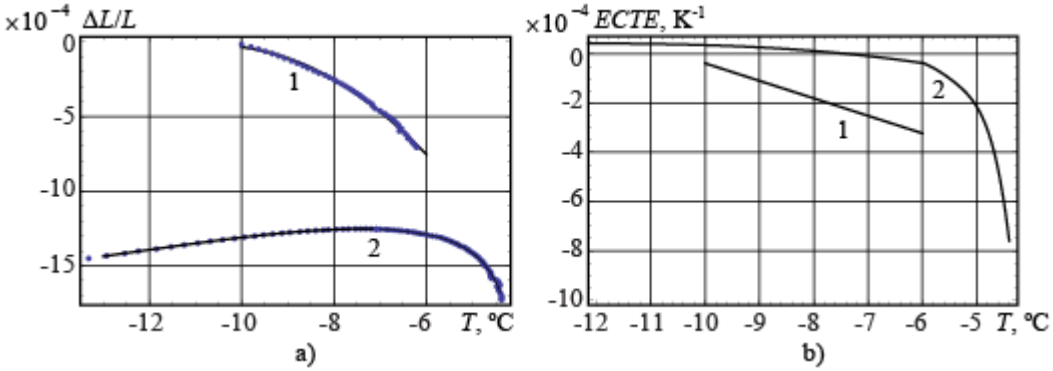

Figure 7. Dependencies of ice sample strain versus ice temperature measured experimentally (blue dots) and their polynomial interpolations (black lines) (a). ECTE versus the ice temperature calculated from the polynomial interpolations of the experimental data.

Experiment on thermo-elastic waves

Experiments to measure thermo-elastic waves were undertaken in the UNIS cold laboratory in 2015. Saline ice samples were prepared from a mixture of sea water and fresh water. Cylindrical samples with inner vertical hole were frozen by adding saline water, layer by layer, into a cylindrical plastic vessel with a fixed coaxial vertical pipe inside. The FBG was fixed by steel plates and bolts on the top and the bottom of the ice sensor, as shown in Fig. 8. The FBG thermistor was placed near the FBG strain sensor. The ice sample was insulated from the environment by foam plastic (Fig 8a).

The upper surface of the sample was subjected to periodical variations of air temperature, caused by the cycle of the fans in the cold laboratory. The period of the air temperature variations was 12 minutes. The inverse wavenumber k^{-1}, calculated from formula (39) and with a wave period of 12 minutes, is around 1cm. This quantity characterizes the depth

of penetration of the air temperature fluctuations into the ice. The FBG strain sensor recorded the vertical deformation of the ice sample created by the temperature oscillations with sampling interval 1s. The air temperature was measured less than 1cm from the ice surface with a Testo 176T4 rod-probe, and on the ice surface with a Testo 176T4 wire-probe (Fig. 9).

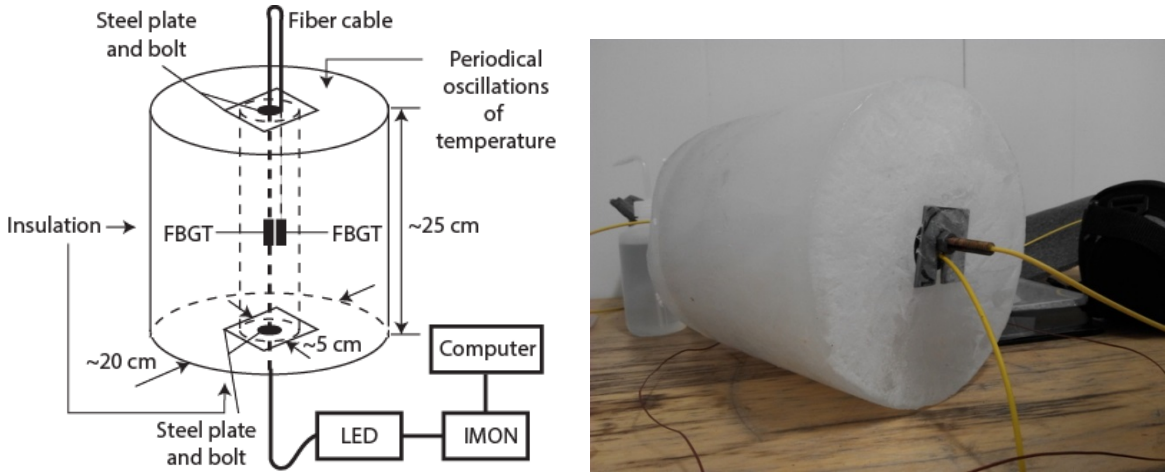

a) b)

Figure 8. Schematic of experiment for detection of TEW (a). Ice sample with optical fiber (b).

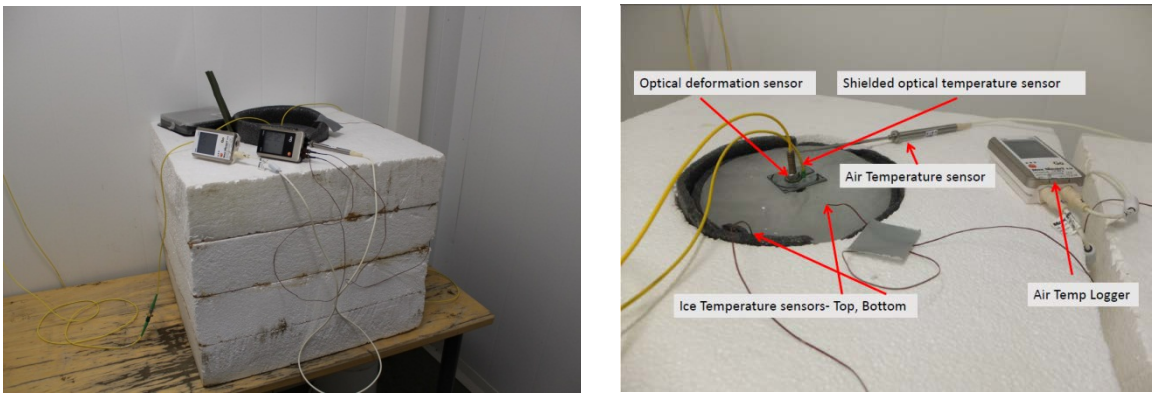

a) b)

Figure 9. Photos of full experiment (a) and sensor installed on the sample (b).

The mean air temperature was kept the same for 5-6 hours to get stable ice temperatures several centimeters below the ice surface, and stable amplitude of thermo-elastic waves at constant mean air temperature. The amplitude of the temperature oscillations measured in the air was 1.8°C, across a range of mean temperatures. Figure 10 shows an example of the temperature and strain record. The general trend of the strain record, and the temperature induced oscillations of strain, are clearly visible. The amplitude of oscillations around 1 μstrain corresponds to the resolution of the FBG strain sensors. A moving average was applied to extract the trend of the strain. The difference between this averaged data and the actual data gives a periodic signal with amplitude proportional to the amplitude A_u of vertical displacements of the ice surface (i.e. the TEW amplitude).

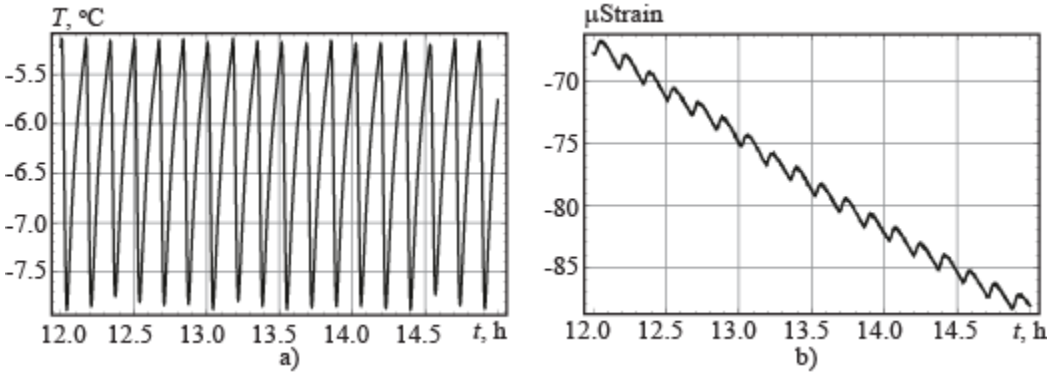

Figure 10. Example of temperature (a) and strain (b) oscillations in ice sample versus the time.

The amplitudes of the temperature oscillations measured with the wire-probe on the ice surface were smaller than the amplitudes measured with the rod-probe in air, and were highly dependent on the nature of the freezing between probe and ice surface. Actual amplitudes of the ice surface temperature are assumed to be between the wire-probe and rod-probe measurements. Therefore we include a calibration coefficient to compare the shape of the experimental and theoretical dependencies of the DT ratio on the mean surface temperature. The theoretical dependence of the DT ratio on the mean surface temperature was calculated using formula (40).

These theoretical dependencies of the DT ratio on the mean ice temperature are shown in Fig. 11a when closed brine pockets are absent (σ_{icp}=0). The values of ice salinity σ_{si} are shown near the lines. Figure 11b shows the theoretical dependencies of the DT ratio on the mean ice temperature when σ_{si} = 5 ppt. The values of ICP salinity σ_{icp} are shown near the lines. One can see that the DT ratios shown in Fig.11a are much smaller than those shown in Fig. 11b. The DT ratios decrease when the mean temperature increases in Fig. 11a, and the DT ratios increase when the mean temperature increases in Fig. 11b. Examples of the DT ratios (as a function of mean temperature) reconstructed from experiments are shown in Fig. 12a for σ_{si}=9ppt by blue dots and for σ_{si}=5ppt by pink dots. These results show increasing DT ratios when the mean temperature increases. This type of behavior is similar to that shown in Fig. 11b. The values of the DT ratios in Fig. 12 are smaller than the values shown in Fig. 11b because only a fraction of the liquid brine is trapped in closed brine pockets of saline ice in the laboratory experiment. The solid lines in Fig. 12a show a (second order) polynomial fit of the DT ratios. Figure 12b shows the dependencies of the ICP salinity on the temperature found from formula (40) after the substitution of the polynomial fits of the DT ratios shown in Fig. 12a. Both of the dependencies demonstrate a decrease of the ICP salinity with increasing temperature.

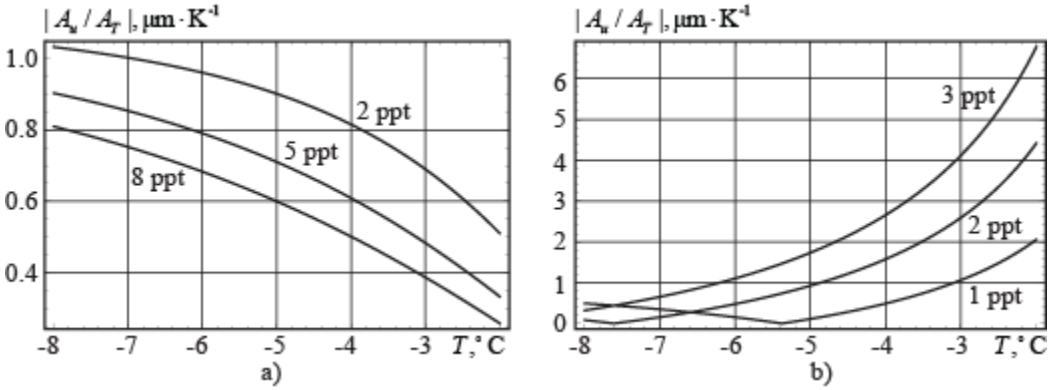

Figure 11. Theoretical dependencies of the DT ratio on temperature, calculated for saline ice of different salinity without closed brine pockets (a) and for saline ice of 5 ppt salinity with closed brine pockets with different ICP salinities (b).

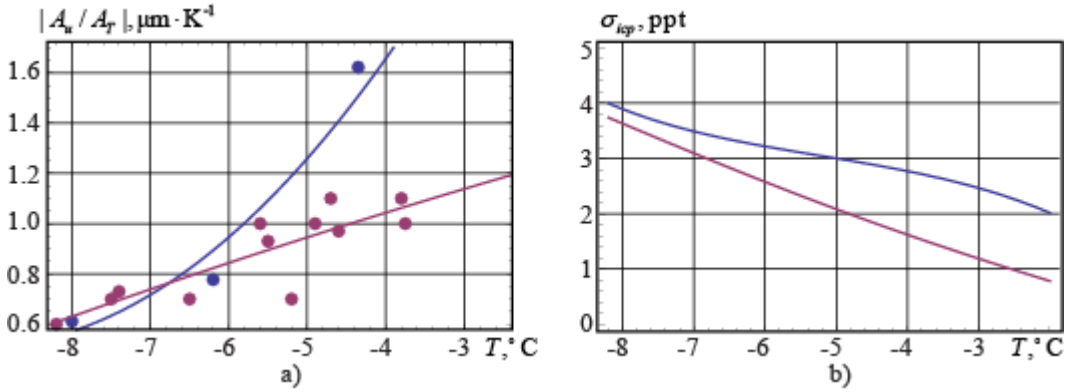

Figure 12. Dependencies of the DT ratio on temperature, found from experiments on thermo-elastic waves (markers show experimental data points and lines show polynomial fits) (a). Solid lines show the dependencies of ICP salinity on temperature, calculated with the polynomial fit of the DT ratios from formula (39) (b). Blue dots and lines correspond to σ_{si}= 9 ppt and pink dots and lines correspond to σ_{si}= 5 ppt.

Conclusions and Discussion

A thermodynamic model of saline ice, accounting for phase changes and liquid brine migration in the porous space, has been formulated, and basic equations derived. It is assumed that sea ice is composed of two intermingled parts: ice with closed brine pockets (ICP), and liquid brine in permeable channels (BPC). The liquid brine content of the ICP is characterized by the ICE salinity σ_{icp} which is lower than the total ice salinity σ_{si}. The brine migration through the permeable channels is described by Darcy's law in the model. The ICP salinity σ_{icp} can be determined from the temperature T and the total ice salinity σ_{si} through an empirical equation. It has been shown that the coefficient of thermal expansion of sea ice, as given by the model, is similar to the coefficient of thermal expansion derived by Malmgren [4] when the sea ice salinity is equal to the ICP salinity.

We have conducted theoretical investigations of the thermal deformations of a sea ice half space caused by periodical changes of the surface temperature. These temperature oscillations penetrate into the ice and cause ice deformations. These are thermo-elastic waves (TEW). We analyzed the dependence of the amplitude of vertical displacements of the ice surface (i.e. TEW amplitude) on the mean ice temperature when the amplitude of the surface temperature oscillations is fixed. It was shown that the TEW amplitude is expected to decrease with increasing mean ice temperature when all the liquid brine is located in permeable brine channels, and σ_{icp}=0. The TEW amplitude increases with increasing mean ice temperature when the ICP salinity is greater than zero (σ_{icp}>0).

We investigated the dependency of the effective coefficient of linear thermal expansion (ECTE) on temperature, in laboratory experiments. Values of ECTE around 5×10^{-5}K^{-1} were found for fresh ice, and these are close to the widely accepted value. Negative values of ECTE were found in samples with salinity of 6ppt and higher. Atypical thermal behavior – contraction with increasing temperature – was observed across several experiments at temperatures higher than -8°C.

The absolute values of the ECTE were lower than those given by Malmgren [4] but can be modelled by assuming that only a part of the liquid brine exists in closed brine pockets. The experimental dependency of ECTE on temperature was compared with theoretical predictions, and a reasonable match was achieved by tuning the ICP salinity σ_{icp}. We find that the ICP salinity (which tells us, effectively, how much brine is in closed pockets and how much in open channels) should be lower than total ice salinity. The amount of salt trapped in closed pockets decreases with the temperature increase. In our experiments it takes of about 60% of total ice salinity when the ice temperature was below -14^{o}C and drops below 20% of total ice salinity when the ice temperature was above -8^{o}C.

In the experiment with a constrained ice sample of 8 ppt salinity, we discovered that the ECTE varies within the same experiment, so that two distinct clusters of strain (and hence trends of ECTE) are visible. Such behavior could be explained by temporal locking and unlocking of BPC, perhaps due to the influence of the constraining pipes. Therefore we think that thermal expansion of saline ice is a highly dynamic process, accompanied by temporal variations of the fraction of closed brine pockets, depending on spatial sizes and confinement of the ice. Numerical simulations of the experiment [9] shown that the maximum value of thermally induced axial displacement of the confined ice sample,

calculated with an elastic model, is similar to the axial displacement of an unconfined sample. If creep is incorporated, the maximum displacement is modelled to increase around 20% (assuming no slip between ice and steel). Frictional sliding between ice and steel may influence the measured thermal expansion in our experiments. This effect should be further studied.

Theoretically derived thermo-elastic waves have been validated in laboratory experiments with saline ice samples. In the experiments we registered periodic elongation and shortening of ice samples, caused by periodic cycles of the air temperature around some mean value. The amplitudes of these thermo-elastic waves increase with increasing room temperature. Within our model, this occurs only when the ice includes some amount of brine in closed pockets ($\sigma_{icp}>0$).

We have managed to reproduce the main trends of the ECTE dependency on temperature, and the dependency of TEW amplitudes on temperature by adjusting ICP salinity σ_{icp}. Phase changes occur at the boundaries of the closed brine pockets, and these phase changes are accompanied by changes of local pressure and deformations due to the 10% difference between ice and brine densities. These stresses are not accounted in the model. The gas content of saline ice [21, 22] may play a role in damping this effect, and the presence of gas content could be incorporated into later models.

Measurements of strain and temperature were performed with Fiber Bragg Grating sensors, which can be recommended as a productive tool for laboratory measurements of the thermo-mechanical properties of saline ice. We were able to perform experiments with samples of various sizes, geometries and configurations; sampling at 1Hz; and with high accuracy and resolution across a temperature range from 0°C to -20°C. The sensors, and their associated hardware and software, were stable and robust. The main experimental complication was in developing techniques to mount the FBG sensors onto the ice samples.

The results in this paper suggest that the some brine within sea ice may be contained in closed pockets, and unable to permeate through the ice under typical pressure differences. This in turn may influence the thermal expansion of sea ice. This work may be of interest to those modelling sea ice thickness and salinity distribution on both local scales and large scales [23, 24].

Additional Information

Dispersion equation

$$\omega = ik^2 / X_T\,,\ X_T\lambda_{si0} = \langle \rho c \rangle_{si0} + \rho_{i0} L_i (A - BC/D)_0 \tag{42}$$

$$A = -\frac{\partial \nu_{icp}}{\partial T} - \frac{\partial \nu_{icp}}{\partial \sigma_{icp}}\frac{\partial \sigma_{icp}}{\partial T} + \nu_{icp}\frac{\partial \nu_{bi}}{\partial T} + \nu_{icp}\frac{\partial \nu_{bi}}{\partial \sigma_{icp}}\frac{\partial \sigma_{icp}}{\partial T}$$

$$B = -\frac{\partial \nu_{icp}}{\partial \sigma_{si}} - \frac{\partial \nu_{icp}}{\partial \sigma_{icp}}\frac{\partial \sigma_{icp}}{\partial \sigma_{si}} + \nu_{icp}\frac{\partial \nu_{bi}}{\partial \sigma_{si}} + \nu_{icp}\frac{\partial \nu_{bi}}{\partial \sigma_{icp}}\frac{\partial \sigma_{icp}}{\partial \sigma_{si}}$$

$$C = \sigma_{si}\left(\frac{\partial \rho_{si}}{\partial T} + \frac{\partial \rho_{si}}{\partial \sigma_{icp}}\frac{\partial \sigma_{icp}}{\partial T}\right) - \left(\rho_b \sigma_b \nu_b + \rho_{icp}\sigma_{icp}\nu_{icp}\right)\frac{\mathrm{K}\alpha_{icp0}}{4G/3 + \mathrm{K}}$$

$$D = \sigma_{si}\left(\frac{\partial \rho_{si}}{\partial \sigma_{si}} + \frac{\partial \rho_{si}}{\partial \sigma_{icp}}\frac{\partial \sigma_{icp}}{\partial \sigma_{si}}\right) + \rho_{si}$$

Instrumentation

Experiments on thermal expansion and measurements of thermo-elastic waves in saline ice were performed with Fiber Bragg Grating (FBG) sensors manufactured in AOS GMBH (Dresden). A Fiber Bragg grating is a periodical index change in the refractive index *n* along an optical silica fiber's core, formed by an interference pattern of two UV laser beams that the fiber is exposed to. With a period of less than 10^{-6}mm, areas of higher *n* alternate with areas of lower *n* while Δn is relatively small ($\Delta n < 0.001$ *at* $n = 1.45$). Due to the index change, each "grating line" reflects a very small portion of the light wave propagating along the fiber, back to the light source. Although a single reflected portion is negligible compared to the transmitted power, the effect becomes noticeable because the amount of "grating lines" in a

conventional FBG is about 4000/mm, and a typical FBG with 10 mm length consists of 40 thousands reflections. If the light's wavelength matches the condition

$$\lambda_{Bragg} = 2 \cdot n_{eff} \cdot \Lambda, \tag{43}$$

where n_{eff} is the fiber's effective index, λ_{Braqq} is the light's wavelength, and Λ is the index change's period, then all reflected light wave portions are propagating "in-phase" and interfere constructively. It is easy to see that λ_{Braqq} will change when the fiber is strained or compressed, whereas the effective refractive index is a material property and thus n_{eff} is sensitive to changes in temperature. This sensitivity of the peak wavelength with respect to thermal and mechanical loads allows the usage of FBG as strain and temperature sensors [25,26].

In our experiment, FBG sensors are practical for measuring the thermal expansion of large samples because, in contrast to standard dilatometers, the fiber can be embedded directly inside the ice sample. FBG thermistor string and strain sensor are shown in Fig. 13. Typical strain resolution for FBG systems is 10^{-6} (1 μstrain) or better, and the accuracy is typically $5 \cdot 10^{-6}$ (5 μstrain). These characteristics are comparable to Michelson Interferometer Laser Dilatometers as used by Johnson and Metzner (1990) and discussed above.

The variation ($\Delta\lambda_{Braqq}$) of the peak wavelength caused by the extension ($\Delta L/L$) and the change of the temperature (ΔT) of the sensor is described by the equation

$$\frac{\Delta\lambda}{\lambda} = GF \cdot \frac{\Delta L}{L} + TK \cdot \Delta T\ , \tag{44}$$

where the gauge factor GF=0.719 and a linear temperature coefficient TK=5.5·10^{-6} are the constants obtained from a calibration cycle for our FBG sensors in standard SMF fiber, within a temperature range from -20^{o} C to 0^{o} C.

The variation of the peak wavelength $\Delta\lambda$ is measured with a spectrometer that receives the reflected signal from the FBG sensor. For the calculation of the strain (($\Delta L/L$) according to formula (40) it is necessary to measure the temperature change (ΔT) at the strain sensor's position in order to compensate TK. The temperature measurements can easily be performed with another FBG sensor protected from mechanical deformation, or alternatively with a thermometer. In our experiments, we used FBG strain sensors with a reference peak wavelength in the vicinity of around 1534 nm, and FBG temperature sensors with a reference peak wavelength in the vicinity of around 1565 nm. The strain and temperature sensors were cascaded in one optical fiber. The FBG measurement system's nominal resolution and accuracy in our experiment was 0.08^{o} C and 0.4^{o} C, respectively.

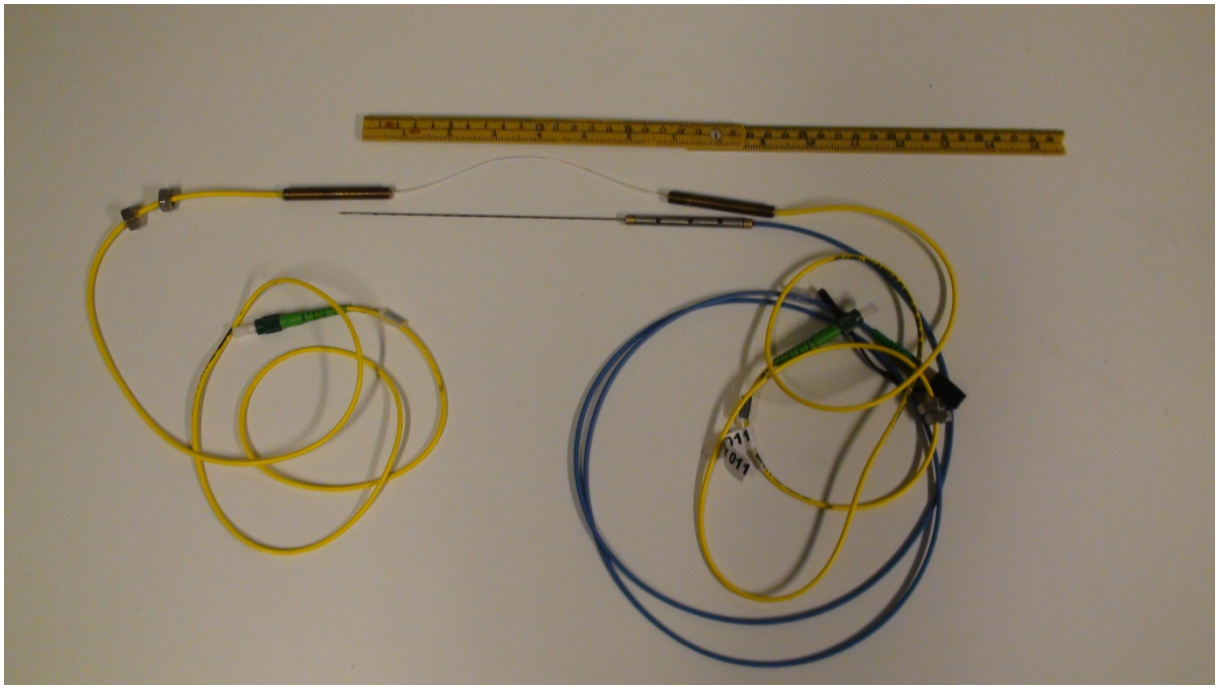

Figure 13. An FBG thermistor string and strain sensor.

Acknowledgments
The authors wish to acknowledge the support of the Research Council of Norway through the SFI SAMCoT and Petromaks2 project Experiments on waves in oil and ice.

Funding Statement
Aleksey Marchenko – Budget funding of the University Centre in Svalbard
Ben Lishman - Budget funding of University College London

Data Accessibility
All manuscripts which report primary data (usually research articles) should include a Data Accessibility section which states where the article's supporting data can be accessed. This section should also include details, where possible, of where to access other relevant research materials such as statistical tools, protocols, software etc. If the data has been deposited in an external repository this section should list the database, accession number and link to the DOI for all data from the article that has been made publicly available, for instance:
DNA sequences: Genbank accessions F234391-F234402 (**http://dx.doi.org/xxxxx**)
Phylogenetic data, including alignments: TreeBASE accession number S9123 (**http://dx.doi.org/xxxxx**)
Climate data and MaxEnt input files: Dryad doi:10.5521/dryad.12311 (**http://dx.doi.org/xxxxx**)

If the data is included in the article's Supplementary Material this should be stated here, for instance:
The datasets supporting this article have been uploaded as part of the Supplementary Material.

Competing Interests
We have no competing interests.

Authors' Contributions
Aleksey Marchenko – formulation of the model, experiments on thermal expansion, experiments on thermo-elastic waves, data processing, drafting the article, final approval of the version to be published.
Ben Lishman – critical analysis of the model equations, experiments on thermal expansion, data processing, drafting the article, revising the article critically for important intellectual content, final approval of the version to be published.

References

1. Johnson J.B., Metzner R.C. 1990. Thermal expansion coefficients for sea ice. *Journal of Glaciology*, 36(124), 343-349.
2.Golden, K.M., Eicken, H., Heaton, A.L., Miner, J., Pringle, D.J., Zhu, J. 2007. Thermal evolution of permeability and microstructure in sea ice. *Geophysical Research Letters*, 34, L 16501.
3. Petterson, O. 1883. On the properties of water and ice. In *Nordenskiold, ed. Vega-expeditionens veisnskapliga iakttagelser*. Bd.2. Stockholm, F. and G. Beijers Forlag, 247-323.
4. Malmgren, F., 1927. On- the properties of sea ice. Tech. Rep. Vol. 1a, Scientific results : The Norwegian North Polar Expedition with the "Maud" 1918-1925, ed. Harald U. Sverdrup, 67pp.
5. Cole, D.M., Shapiro, L.H., 1998. Observations of brine drainage networks and microstructure of first-year sea ice. *Journal of Geophysical Research*, 103(NC10), 21,739-21,750.
6.Cox, G.F.N. 1983. Thermal expansion of saline ice. *Journal of Glaciology*, 29(103), 425-432.
7. Marchenko, A., Thiel, T., Sukhorukov, S. 2012. Measurements of Thermally Induced Deformations in Saline Ice with Fiber Bragg Grating Sensors. *Proceedings of 21st IAHR International Symposium on Ice "Ice Research for a Sustainable Environment"*, Li and Lu (ed.), Dalian University of Technology Press, Dalian, T07105, 9pp.
8. Marchenko, A., Wrangborg, D., Thiel., T. 2013. Using distributed optical fiber sensors based on FBGs for the measurement of temperature fluctuations in saline ice and water on small scales. *Proceedings of POAC13*, Espoo, Finland, POAC13-134.
9. Lishman, B., Marchenko, A. 2014. An investigation of relative thermal expansion and contraction of ice and steel. *Proc. of the 22th IAHR Symposium on Ice*, Singapore, paper 173.
10. Marchenko, A., Lishman, B. 2015. Properties of thermo-elastic waves in saline ice. *Proceedings of POAC15*, Trondheim, Norway, POAC15-164, 11 pp.
11. Schwerdtfeger, P. 1963. The thermal properties of sea ice. *Journal of Glaciology*, 4 (36), 789–807.

12. Spiegelman, M., 1993. Flow in deformable porous media. Part 1 Simple analysis. *J. Fluid. Mech*., 247, 17-38.
13. Collins, R., 1961. Flow of fluids through porous materials. New York, Reinhold Pub, Corp., 270 p.
14. Schulson, E.M., Duval, P., 2009. Creep and fracture of ice. Cambridge University Press, 416 p.
15. Pounder, E.R., 1965. The physics of ice. Oxford, etc., Pergamon Press.
16. Zhu, J., Jabini, A., Golden, K.M., Eicken, H., Morris, M. 2006. A network model for fluid transport through sea ice. *Annals of Glaciology*, 44, 129-133.
17. Landau, L.D., Lifshitz, E.M., 1970. Theory of Elasticity, Oxford, Pergamon Press, 165 p.
18. Gammon, P.H., Kiefte, H., Clouter, M.J., Denner, W.W., 1983. Elastic constants of artificial and natural ice samples by Brillouin spectroscopy. *Journal of Glaciology*, 29, 433-460.
19. Boley, B.A., Weiner, J.H., 1960. Theory of thermal stresses. New York, John Wiley and Sons, Inc., 586 p.
20. Landau, L.D., Lifshitz, E.M., 1977. Fluid Mechanics, Oxford, Elsevier Ltd., 539 p.
21. Cox G.F.N., Weeks, W.F., 1983. Equations for determining the gas and brine volumes in sea-ice samples. *Journal of Glaciology*, 29(102), 306-316.
22. Tison, J.-L., Haas, C., Gowing, M.M., Sleewaegen, S., Bernard, A., 2002. Tank study of physico-chemical controls on gas content and composition during growth of young sea ice. *Journal of Glaciology*, 48(161), 177-191.
23. Vancoppenolle, Martin, Thierry Fichefet, and Hugues Goosse. "Simulating the mass balance and salinity of Arctic and Antarctic sea ice. 2. Importance of sea ice salinity variations." *Ocean Modelling* 27, no. 1 (2009): 54-69.
24. Vancoppenolle, Martin, Thierry Fichefet, and Cecilia M. Bitz. "Modeling the salinity profile of undeformed Arctic sea ice." Geophysical Research Letters 33, no. 21 (2006).
25. Rao, Y.J., 1997. In-fiber Bragg grating sensors. *Measurement Science and Technology*, 8(4), Sci. Technol., 8, 355-376.
26. Othonos, A., Kalli, K., 1999. Fiber Bragg Gratings: Fundamentals and Applications in Telecommunications and Sensing. Artech House.